Nuclear star cluster formation in energy-space

Nathan W. C. Leigh[1,2], Iskren Y. Georgiev[3], Torsten Böker[3], Christian Knigge[4], Mark den Brok[5] ⋆

[1] *Department of Astrophysics, American Museum of Natural History, Central Park West and 79th Street, New York, NY 10024*
[2] *Department of Physics, University of Alberta, CCIS 4-183, Edmonton, AB T6G 2E1, Canada*
[3] *European Space Agency, Space Science Department, Keplerlaan 1, 2200 AG Noordwijk, The Netherlands*
[4] *School of Physics and Astronomy, University of Southampton, Highfield, Southampton, SO17 1BJ, United Kingdom*
[5] *Department of Physics and Astronomy, University of Utah, 115 South 1400 East, Salt Lake City, UT 84112, USA*

12 August 2018

ABSTRACT

In a virialized stellar system, the mean-square velocity is a direct tracer of the energy per unit mass of the system. Here, we exploit this to estimate and compare root-mean-square velocities for a large sample of nuclear star clusters and their host (late- or early-type) galaxies. Traditional observables, such as the radial surface brightness and second-order velocity moment profiles, are subject to short-term variations due to individual episodes of matter infall and/or star formation. The total mass, energy and angular momentum, on the other hand, are approximately conserved. Thus, the total energy and angular momentum more directly probe the formation of galaxies and their nuclear star clusters, by offering access to more fundamental properties of the nuclear cluster-galaxy system than traditional observables. We find that there is a strong correlation, in fact a near equality, between the root-mean-square velocity of a nuclear star cluster and that of its host. Thus, the energy per unit mass of a nuclear star cluster is always comparable to that of its host galaxy. We interpret this as evidence that nuclear star clusters do not form independently of their host galaxies, but rather that their formation and subsequent evolution are coupled. We discuss how our results can potentially be used to offer a clear and observationally testable prediction to distinguish between the different nuclear star cluster formation scenarios, and/or quantify their relative contributions.

Key words: galaxies: nuclei – galaxies: formation - galaxies: photometry – methods: statistical – galaxies: kinematics and dynamics – galaxies: evolution.

1 INTRODUCTION

Recent studies have revealed that nuclear star clusters (NSCs) occur commonly in galaxies of every type (e.g. Binggeli, Sandage & Tarenghi 1984; Kormendy & Kennicutt 2004). These massive and compact star clusters occupying the centres of galaxies are characterized by small effective radii and high central surface brightnesses that help to distinguish them from the surrounding bulge and disk.

Several theories have been proposed to explain the origins of NSCs, but two in particular have emerged as leading scenarios. The first invokes gas accretion at the centres of galaxies to form stars (e.g. McLaughlin, King & Nayakshin

2006; Nayakshin, Wilkinson & King 2009). The second postulates successive mergers of globular clusters (GCs) that spiral into the galactic centre due to dynamical friction (e.g. Tremaine, Ostriker & Spitzer 1975; Quinlan & Shapiro 1990; Gnedin, Ostriker & Tremaine 2014). Several authors have used (primarily N-body) simulations to succesfully reproduce some of the observed features of NSCs formed via this mechanism, including their effective radii and central velocity dispersions (e.g. Capuzzo-Dolcetta & Miocchi 2008). For example, Gnedin, Ostriker & Tremaine (2014) recently modeled the effects of dynamical friction on the orbits of GCs within their host galaxies, in conjunction with the underlying dynamical evolution of the infalling clusters, including mass loss (due to both stellar evolution and tidal stripping) and tidal disruption. The model successfully reproduces the observed features of NSCs in both late- and early-type galaxies.

Whatever the dominant formation scenario for NSCs,

⋆ E-mail: nleigh@amnh.org (NL); tboeker@cosmos.esa.int (TB); C.Knigge@soton.ac.uk (CK); iskren.y.g@gmail.com (IG); den-brok@physics.utah.edu

the evidence suggests that it is an on-going process. The nuclei of late-type disk galaxies have been shown to be populated by stars spanning a wide range of ages, with some members being as young as a few tens of Myrs (e.g. Long, Charles & Dubus 2002). Many authors have suggested that this is indicative of episodic star formation that has occurred over an extended period of time. Proponents of the GC infall scenario, on the other hand, have argued that the young ages of some of the stars can be accounted for if star clusters spanning a range of ages were accreted. In at least the Milky Way, most young star clusters are of relatively low-mass in present-day star forming regions. On the other hand, Nguyen et al. (2014) found several super star clusters at the centre of Henize 2-10, a blue compact dwarf galaxy with an on-going starburst at its centre. The authors argue that many of these young massive ($\sim 10^6$ M$_\odot$) clusters have very short dynamical friction time-scales, suggesting that this may be a rare snapshot of nuclear star cluster formation (via the infall of young massive clusters) around a pre-existing super-massive black hole. Regardless, the evidence suggests that GC infall cannot be the whole story in at least some NSCs, and that in at least these cases some in situ star formation has occurred. For example, this was illustrated by Hartmann et al. (2011) for the nearby disc galaxies NGC 4244 and M33 using both observations and dynamical models of the NSCs at their centres. The authors argue that gas dissipation is required to account for $\gtrsim 50\%$ of these NSCs' masses.

In this paper, we calculate and compare the mean-square velocities of NSCs and their host galaxies, which we use as proxies for energy per unit mass in these systems. Traditional observables, including the radial surface brightness and second-order velocity moment profiles, vary on relatively short time-scales due to episodes of matter infall and/or star formation. Meanwhile, the total mass, energy and angular momentum remain approximately conserved. Total energy and angular momentum are decided by the various processes that go into forming NSCs and their host galaxies, whereas traditional observables are also affected by any subsequent or secondary evolution that occurs in energy- and angular momentum-space post-formation. Thus, the total energy and angular momentum more directly probe the formation of galaxies and their nuclear star clusters, by offering access to more fundamental properties of the nuclear cluster-galaxy system than traditional observables. However, we caution that our analysis relies on the same observable quantities to calculate mean-square velocities and that we make the additional assumption of virial equilibrium, which introduces some further uncertainty. Regardless, as we will illustrate, the comparison is nonetheless instructive. In particular, there is a priori no reason to expect that the formation and subsequent time evolution of NSCs should be coupled to their host galaxies in energy- and angular momentum-space. If NSCs and their hosts form independently[1], then they should remain independent in energy- and angular momentum-space at the present-day. Our re-

sults suggest that NSCs *are* coupled to their hosts in energy-space. We subsequently explore the physical processes that could produce such a correlation and, based on this, propose a means of also using total angular momentum to further constrain NSC formation. In Section 2, we describe the requisite theoretical background. We present the data we use in this paper to calculate the root-mean-square velocities in Section 3, both for early- and late-type galaxies. Our results are presented in Section 4. In Section 5, we discuss the significance of our results for different NSC formation scenarios, and conclude in Section 6.

2   BACKGROUND

In this section, we describe the necessary theoretical background. The purpose here is to motivate our choice for calculating mean-square velocities for both the central NSCs and their host galaxies. As we will show, the mean-square velocity is a proxy for the energy per unit mass of the system, assuming virial equilibrium. The evolution in energy- and angular momentum-space is what determines the balance between the total system mass, half-mass radius and root-mean-square velocity (see Equations 4 and 5), via the virial theorem. Thus, the total energy and angular momentum, which are initially determined by the various formation processes and are subsequently conserved in time, are fundamental to determining the observed parameters of a self-gravitating system, which are not time-independent. Naively, there is no reason to expect that the formation and subsequent time evolution of NSCs in energy- and angular momentum-space should be coupled to their host galaxies. If NSCs and their hosts form independently, then the evolution in energy- and angular momentum-space should proceed independently, first on a crossing time-scale (virialization) and then on a relaxation time-scale (two-body relaxation in energy-space and resonant relaxation in angular momentum-space; although the two-body relaxation time-scale tends to exceed a Hubble time in both NSCs and, especially, their host galaxies) (e.g. Merritt 2013). Intriguingly, however, we will show that there is a strong (nearly) linear correlation, and in fact a near equality, between the energy per unit mass (via the mean-square velocity) of NSCs and that of their host galaxies.

We assume virial equilibrium for all NSCs and host galaxies. The scalar virial relation yields 2E = -2K = W, where E is the total system energy, K is the total kinetic energy and W is the total potential energy. The kinetic and potential energies are, respectively:

$$K = \frac{1}{2} M v_{\rm rms}^2 \tag{1}$$

and

$$W = -\frac{GM^2}{r_{\rm g}}, \tag{2}$$

where $v_{\rm rms}$ and $r_{\rm g}$ are the root-mean-square stellar speed and the gravitational radius, respectively, and M is the total stellar mass. It follows from the virial theorem that the mean-square velocity is given by:

$$v_{\rm rms}^2 = \frac{|W|}{M} \approx \frac{0.4GM}{r_{\rm h}}, \tag{3}$$

---

[1] For example, while we might naively expect that at least *some* correlation should be present in energy-space in most formation scenarios, violent or rapid episodes of mass growth in NSCs could erase it.

where the last (approximate) equality holds for many simple stellar systems (Spitzer 1969), and r_h is the median radius (or half-mass radius) which is related to the gravitational radius via $r_h \sim 0.4 r_g$. In general, the gravitational radius is related to the system half-mass radius via a multiplicative constant that depends on the gravitational potential, or $r_g = \alpha_r r_h$. For example, for a spherically symmetric stellar system, we have $r_g = 2 r_h$ (Jaffe 1983). Throughout this paper, we assume $r_g = 2 r_h$ (i.e. $\alpha_r = 2$ in Equation 5) for all NSCs as well as for the bodies of all early-type galaxies, and $r_g = r_h$ (i.e. $\alpha_r = 1$) for the bodies of all late-type galaxies (e.g. Binney & Tremaine 1987) (see below).

We calculate the mean-square velocities for NSCs and their host galaxies using Equations 1 and Equation 2. For the NSCs, we use (Binney & Tremaine 1987):

$$v_{\mathrm{rms,NSC}}^2 = \frac{GM_{\mathrm{NSC}}}{2 r_{\mathrm{NSC}}}, \quad (4)$$

and for the host galaxies we use:

$$v_{\mathrm{rms,Gal}}^2 = \frac{GM_{\mathrm{Gal}}}{\alpha_r f_g r_{\mathrm{Gal}}}, \quad (5)$$

where M_{NSC} and M_{Gal} are, respectively, the total stellar (or baryonic) mass of the NSC and host galaxy, f_g is the baryonic mass fraction inside r_{Gal}, and r_{NSC} and r_{Gal} are the effective or projected half-light radii r_h of the NSC and host galaxy, respectively, which we use as proxies for the 3-D half-mass radii (see below). These masses and radii are derived from the observations as described in Sections 3.1 and 3.2. We further assume a constant dark matter mass fraction (but see Section 4 for further discussion of this issue and its effects on our results) inside the effective radius r_h for all galaxies, corresponding to a baryonic mass fraction $f_g = 0.87$ (Cappellari et al. 2013a,b; Toloba et al. 2014a,b).

In practice, kinematical data (i.e. the two terms in Equation 6 below, which correspond to the second-order velocity moments projected along the line of sight) are difficult to obtain. Consequently, very few such measurements have been provided in the literature (e.g. Busarello, Longo & Feoli 1992; Chae, Bernardi & Kravstov 2014; Toloba et al. 2014a,b). This is the reason we calculate root-mean-square velocities indirectly from the virial theorem using the total system mass and the half-light or effective radius, as opposed to using the directly measured second-order velocity moments.

How does the root-mean-square velocity calculated from the virial theorem relate to what is actually observed? Similarly to r_g, the root-mean-square velocity v_{rms} is not measured directly, but rather indirectly via the observed second-order velocity moment $v^2 + \sigma^2$, where v and σ are the observed mean stellar velocity (i.e. the mean velocity of ordered bulk motion) and velocity dispersion, respectively. To obtain v_{rms}^2 from the observed velocity moments projected along the ling-of-sight, we would need to include multiplicative factors, or (Busarello, Longo & Feoli 1992):

$$v_{\mathrm{rms}}^2 = \alpha_v v^2 + \alpha_\sigma \sigma^2 \quad (6)$$

The constants α_v and α_σ are determined by the gravitational potential and the angle of inclination relative to the line-of-sight. For example, $\alpha_v = 1$ and $\alpha_\sigma = 3$ in the case of an isothermal sphere, which is spherically symmetric (Emsellem et al. 2007). For a non-spherical potential, how-

ever, the angle of inclination must be accounted for when measuring the parameters α_v and α_σ.

3 THE DATA

In this section, we describe the data used to compile our samples of both early- and late-type galaxies, beginning with the former. We summarize in Appendix A all NSC galaxy masses and root-mean-square velocities calculated from these data. This is done in Tables A1, A2 and A3 for each of the late-type, Virgo Cluster and Coma Cluster samples, respectively.

3.1 Early-type galaxies

For our analysis of early-type galaxies, we use data from the Virgo and Coma Cluster Surveys. Beginning with the former, we use data for 47 nucleated early-type galaxies observed during the *Advanced Camera for Surveys* Virgo Cluster Survey (ACSVCS, Cote et al. 2004). We reject five galaxies from the original sample of Cote et al. (2006) in which the apparent NSCs are significantly offset from the galaxy's photocentre and therefore, as discussed by Cote et al. (2006), may well be globular clusters that only appear to reside close to the nucleus due to a chance projection (Leigh, Böker & Knigge 2012). We also discard four galaxies with extended nuclei (Graham 2012; Scott & Graham 2013), which are more accurately described as nuclear disks (Balcells 2007), from our sample.

In order to obtain estimates for the stellar masses, we use the apparent z-band magnitudes, (g-z) colors, and half-light radii for both NSCs (from Cote et al. 2006) and host spheroids (from Ferrarese et al. 2006). In order to convert to absolute magnitudes and physical radii, we obtain distances to individual galaxies from Tonry et al. (2001) and Blakeslee et al. (2002) wherever possible, and for galaxies not in the catalogue of Tonry et al. (2001) we adopt a distance of 16.52 Mpc (Cote et al. 2006). We also need to multiply the respective z-band luminosities by an appropriate mass-to-light ratio. We use the empirically calibrated mass-to-light ratios provided by Bell et al. (2003), accounting for the (g-z) color of NSC and spheroid, respectively. We note here that, given the morphological types of the sample galaxies (E, S0, dE, dS0, and dE,N), their stellar spheroids can be expected to be virialized, and to have little or no current star formation activity. This justifies use of a single (colour-dependent) mass-to-light ratio for each galaxy spheroid in order to derive its stellar mass. Approximate error bars for the NSC masses were calculated using the 0.041 mag uncertainty quoted by Cote et al. (2006).

We also use data for 53 nucleated low-mass early-type galaxies observed during the Coma *Advanced Camera for Surveys* Cluster Survey (Carter et al. 2008; den Brok et al. 2014). We include all galaxies in the sample designated as possible members or better. However, we also check our derived scaling relations without including galaxies listed as possible members, since here membership is not certain. Our results turn out to be insensitive to the adopted inclusion criterion. To calculate the NSC and host galaxy masses, we use the corresponding F814W magnitudes. Unlike with the Virgo Cluster sample, we do not have colour information to calculate empirically-calibrated mass-to-light corrections

for the stellar population. Thus, we assume a mass-to-light ratio of 2 for all NSCs and host galaxies to correct for the unseen component of the stellar mass distribution. This is a reasonable assumption for at least the Coma Cluster, since with only a few exceptions, the colour distribution is very narrow (den Brok et al. 2014).

3.2   Late-type galaxies

For our analysis of late-type galaxies, we compiled a sub-sample of 69 galaxies compiled from the sample of Georgiev & Böker (2014), for which there are measurements of their PEtrosian radii in the 10th SDSS data release[2]. These are nearby ($\lesssim 40$ Mpc), mostly low-inclination spirals. We calculate the total galaxy luminosity and its effective radius using their SDSS Petrosian measurements following the prescription given in Graham et al. (2005) (their Sections 3.2 and 3.3, and equations 5 and 6). To obtain masses for these *nuclear star clusters*, we use the luminosities measured from the flux within the best-fitting King model of a given concentration index (as provided in Georgiev & Böker (2014)), multiplied by a suitable mass-to-light correction obtained using the Bruzual & Charlot (2003) simple stellar population models for solar metallicity and a Kroupa (2001) initial mass function. We use the available colour information given by the various combinations of the most reliable and well-calculated filters, namely $F450W$, $F555W$, $F606W$ and $F814W$. All available colours are matched to the respective colours of the Bruzual & Charlot (2003) models, and then a median mass-to-light ratio is calculated for all colours (for more details see Georgiev et al. 2015, in preparation). For the *galaxy* luminosities and sizes, we use the z-band Petrosian magnitudes and Petrosian effective radii given in the tenth data release of the SDSS database, which correspond approximately to the half-light radii of the galaxies. The luminosities are converted to masses using the g- and z-band Petrosian magnitudes along with the Bell et al. (2003) empirically-calibrated mass-to-light ratio colour-corrections.

4   RESULTS

The top panels in Figures 1, 2 and 3 show the relation between nuclear cluster mass and the mass of its host galaxy for all early- and late-type galaxies. The dashed lines have slopes of unity and are shifted along the y-axis to approximately coincide with the distribution of data points in each panel. Lines of best-fit are shown for all samples by the solid lines, found by performing weighted least-square fits to the data. All fit parameters are summarized in Table 1. In all samples, the intrinsic dispersion in the data exceeds the uncertainties on the individual data points. This is partly because, in some galaxies, the calculated uncertainties are too small to be representative of the true underlying uncertainties in the measurements (see Tables A1, A2 and A3 in Appendix A). This is due to the fact that we do not always have errors for both the masses and radii used in our calculations of the root-mean-square velocities. To account for the artificially small error bars, uncertainties on the fit

parameters are found by adding (in quadrature) an additional constant term σ_{int} to the uncertainties on both the NSC and host galaxy masses, and forcing the resulting reduced chi-square of the fit to be unity. Hence, the term σ_{int} is effectively a free parameter in our fits, and is set by the condition $\chi_{\mathrm{red}}^2 = 1$. This increases the uncertainties on the fit parameters to more realistically represent the data. We also divide all galaxy masses by 10^9 M$_\odot$, which is approximately equal to the sample means, in order to minimize the uncertainties on the y-intercepts of our lines of best-fit. For the Virgo Cluster sample we find a slope of 1.74 ± 0.28 (Virgo), whereas for the Coma Cluster and late-type samples we find clearly sub-linear slopes of 0.68 ± 0.10 (Coma) and 0.55 ± 0.08 (late-types). The y-intercepts are 6.47 ± 0.07 (late-types), 6.17 ± 0.13 (Virgo) and 7.01 ± 0.06 (Coma). For comparison, we also perform bootstrapped maximum likelihood non-symmetric error-weighted fits (without adding an intrisinc dispersion term to the uncertainties on the individual data points). In all but the late-type sample, the derived fit parameters are consistent with our previous estimates to within the uncertainties.[3] The slopes for the late-type, Virgo and Coma samples are, respectively, $0.55^{+0.05}_{-0.08}$, $1.92^{+0.02}_{-0.53}$ and $0.79^{+0.08}_{-0.25}$. The corresponding instrinsic scatter estimates are, respectively, $0.211^{+0.004}_{-0.005}$, $0.203^{+0.005}_{-0.005}$ and $0.193^{+0.004}_{-0.005}$. The intrinsic scatter and its uncertainty are found following Jeffreys (1946) and based on Bayesian probability theory, such that the intrinsic dispersion is invariant to rescalings of the problem.

As seen in Figure 1, the fit is poor for the late-type sample. This is due to the presence of ~ 10 significant outliers at the low galaxy mass end of the distribution, many of which have NSCs that are nearly as massive as their host galaxies. Hence, these outliers are in part an artifact of having only included the stellar mass in our estimates for the total galaxy masses, and not the gas mass. In late-type galaxies, this effect can be significant. If the gas mass in these outliers is included in the estimates for their total masses, these data points shift to the right in Figure 1, and it becomes apparent that even these NSCs are only $\lesssim 1\%$ the mass of their host galaxy. Additionally, previous studies have shown that, in at least early-type galaxies, the dark matter mass fraction decreases with increasing galaxy mass or Sersic index (e.g. Cappellari et al. 2006; Forbes et al. 2008). For example, Toloba et al. (2014b) recently illustrated that an anti-correlation exists between f_{DM} (within the effective radius) and total galaxy luminosity for a sample of 39 dwarf early-type galaxies in the Virgo Cluster. This effect is not included in our fits, and should also contribute to increasing the slopes of our lines of best-fit (i.e. closer to unity in the Coma Cluster and late-type samples).

The bottom panels in Figures 1, 2 and 3 show the relation between nuclear cluster root-mean-square velocity and the root-mean-square velocity of its host galaxy, calculated using Equations 4 and 5, respectively. As before,

---

[3] The maximum likelihood method used here is the same as in Georgiev et al. (2015, in preparation), where it is described in more detail. The fit reported here for the late-type sample is taken from Georgiev et al. (2015, in preparation), which uses a much larger sample of 247 late-type galaxies. This accounts for the smaller uncertainties on the fit parameters, compared to the Virgo and Coma Cluster samples.

---

[2] http://cas.sdss.org/dr10/en/home.aspx

Table 1. Parameters for all lines of best-fit for the late-type, Virgo and Coma samples. Each table entry is given in the form (α; β), where α and β are the slope and y-intercept, respectively.

Parameter	$\log M_{NSC} = \alpha \log (M_{gal}/10^9) + \beta$	$\log v_{rms,NSC} = \alpha \log (v_{rms,gal}/40) + \beta$
Late-type	0.55 ± 0.08; 6.47 ± 0.07	0.85 ± 0.13; 0.16 ± 0.25
Virgo	1.74 ± 0.28; 6.17 ± 0.13	1.34 ± 0.17; -0.78 ± 0.33
Coma	0.68 ± 0.10; 7.01 ± 0.06	0.58 ± 0.11; 0.61 ± 0.16

lines of best-fit (solid lines) are obtained from a weighted least-squares fit to the data. The uncertainties on the fit parameters are once again found by accounting for the intrinsic dispersion and forcing a reduced chi-square of unity. In the Virgo Cluster and late-type samples, the slopes are consistent with being linear to within two standard deviations, or 1.34 ± 0.17 (Virgo) and 0.85 ± 0.13 (late-type), respectively. In the Coma Cluster sample, however, the slope is sub-linear, or 0.58 ± 0.11. With these slopes, we find y-intercepts of -0.78 ± 0.33 (Virgo), 0.61 ± 0.16 (Coma) and 0.16 ± 0.25 (late-types). Intriguingly, in both the late-type and Virgo Cluster samples, the slopes shift closer to unity relative to the corresponding slopes in Figures 1 and 2. Again, for comparison, we perform bootstrapped maximum likelihood non-symmetric error-weighted fits, and find that all of these fits are consistent with those presented above to within one standard deviation. For the late-type, Virgo and Coma Cluster samples, we find slopes of, respectively, $0.96^{+0.01}_{-0.45}$, $2.13^{+0.20}_{-1.09}$ and $1.05^{+0.47}_{-0.99}$. The corresponding instrinsic scatter estimates are, respectively, $0.178^{+0.002}_{-0.005}$, $0.182^{+0.004}_{-0.005}$ and $0.182^{+0.006}_{-0.004}$. Note that these intrinsic scatter values are comparable to, albeit slightly smaller than, those for the corresponding fits for the M_{gal}-M_{NSC} relations discussed above.

The bottom panels in Figures 1, 2 and 3 suggest that, to within an order of magnitude, NSCs have roughly the same root-mean-square velocity, and hence energy per unit mass, as their host galaxies. This is the case despite sub-linear slopes for the Coma Cluster sample. For example, the fit for the Coma Cluster sample predicts NSCs at low galaxy masses that have higher root-mean-square velocities than their hosts. However, the distribution of galaxy masses, and root-mean-square velocities, is narrow for the Coma Cluster sample, so we do not actually observe any NSCs with v_{rms} values much higher than their hosts (i.e. by more than order of magnitude).

5 DISCUSSION

In this section, we discuss the significance of our results for NSC formation.

5.1 Energy per unit mass

First, we re-iterate a connection between the root-mean-square velocity at the half-light radius and the energy per unit mass of the system. From Equations 1 and 2, energy per unit mass scales as $E/M \propto v_{rms}^2 \propto M/\alpha_r r_g$. Therefore, if a given NSC has about the same v_{rms} as its host galaxy (within r_h), then both systems have approximately the same energy per unit mass. As mentioned earlier, this result is highly unlikely if NSCs form independently of their host galaxies. Our
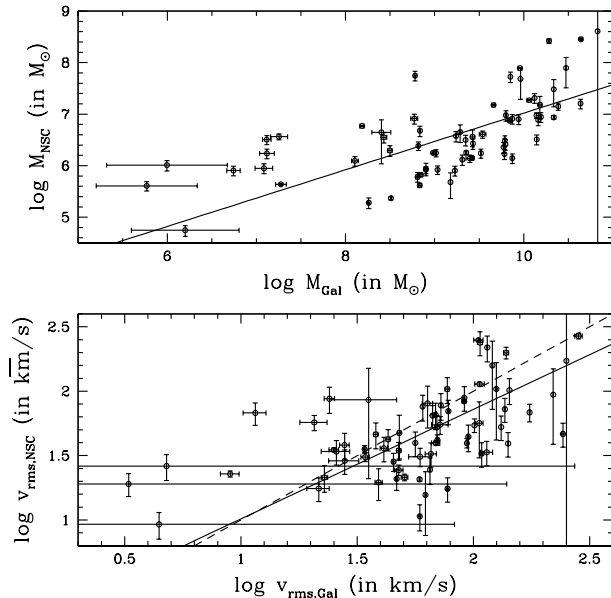
Figure 1. The top panel shows the relation between the stellar mass of NSCs and that of their host galaxies for our sample of late-type galaxies. The bottom panel shows the relation between the stellar root-mean-square velocity for NSCs (Equation 4) and the root-mean-square velocity (Equations 5) of the host galaxy. The solid lines show the corresponding lines of best fit given in Table 1. The dashed line in the bottom panel shows the one-to-one line.

results are consistent with this general picture, since the fit parameters and instrinsic scatter we obtain from our statistical analysis suggest that, in all of the late- and early-type samples considered here, the relation between NSC root-mean-square velocity and that of its host is as statistically significant as the underlying relation between NSC mass and host galaxy mass. However, given the uncertainties inherent to our analysis, this issue should be re-visited when better data become available.

Why do NSCs have roughly (to within an order of magnitude) the same energy per unit mass as their host galaxy? Said another way, our results illustrate that the average star in a nuclear star cluster has roughly the same kinetic energy (and hence total energy, by the virial theorem) as the average non-cluster star in the host galaxy. One interpretation of this result is that NSCs were effectively formed from stars taken directly from the host galaxy, while conserving energy. Hence, in this picture, galaxies form first, and then their NSCs subsequently form from some small piece of their host galaxy bodies. From our perspective, this scenario seems to
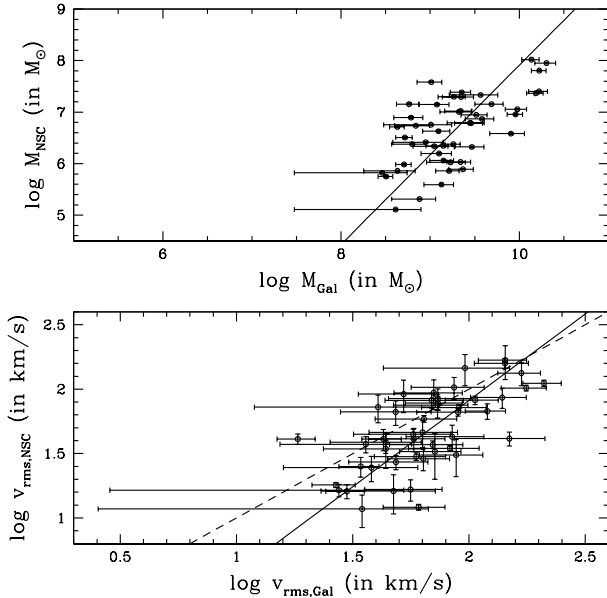
Figure 2. Same as Figure 1 but for the Virgo Cluster sample.
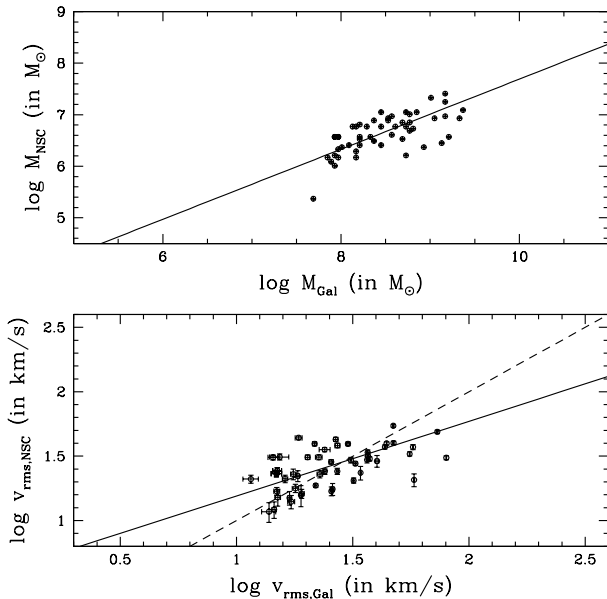
Figure 3. Same as Figure 1 but for the Coma Cluster sample.

be the simplest physically-motivated picture that is consistent with our results. However, it is by no means the only interpretation. For example, it is conceivable that NSCs and their host galaxies form with *different* root-mean-square velocities, and then somehow evolve over time toward a common root-mean-square velocity. However, we are unaware of any physical mechanism that might contribute to such a trend.

5.2 Implications for NSC formation and evolution

Our result can be understood within the framework of both the GC infall and in situ star formation models for NSC formation. For example, consider the GC infall model for NSC formation in a host galaxy with constant circular velocity at all radii (i.e. both inside and outside the effective radius r_h), an idealized assumption we will return to below. The key point is that an infalling GC (on roughly a circular orbit) that has just reached the nucleus due to dynamical friction will have approximately the same velocity relative to the centre of the galaxy as it did several kiloparsecs out. Hence, when stars orbiting within the GC have reached the galaxy centre, their velocities (relative to the galaxy centre of mass) remain similar to the circular velocity at or beyond r_g. It follows that, when the inspiraling GC reaches the galaxy's centre and becomes part of the central nuclear cluster, the energy coming from the bulk motion of the infalling GC is converted to internal thermal energy within the nuclear cluster itself. That is, for a stationary observer at the centre of the galaxy, the centre of mass of the orbiting *cluster* transitions from having a net velocity roughly equal to the circular velocity to having zero net velocity, whereas the *stars within the cluster* always orbit the galaxy centre of mass at the circular velocity. Thus, for galaxies with a constant circular velocity inside the effective radius, this predicts a linear relationship between the energy per unit mass in the central NSC and that of its host galaxy (or, equivalently, a linear relation between the root-mean-square velocity of the central NSC and that of its host, at all radii inside r_g).

Next, consider the in situ star formation scenario for NSC formation, again in a host galaxy with constant circular velocity at all radii. Ignoring radiation losses, we would naively expect a similar picture as outlined for the GC infall model. That is, the gas should reach the central NSC with the same velocity as it had several kiloparsecs out, creating a disk (assuming a preferred plane of accretion) of star-forming gas with a circular velocity that roughly matches that of its host (ignoring any central SMBH). We caution, however, that the picture is potentially more complicated within the framework of the in situ star formation model for NSC formation. This is because, when infalling gas filaments collide with the forming nucleus, shocks can develop that will radiate energy away and lower the energy per unit mass of the central NSC relative to its host. Thus, at least in the ideal case of a collisionless star-forming gas, we expect a central NSC with roughly the same energy per unit mass as its host in galaxies with a constant v_c at all radii, just as in the GC infall model.

The assumption of a constant circular velocity as a function of galactocentric radius is, to first-order, consistent with the observations for most galaxies in our samples (ignoring the innermost regions near the galactic centre). First, consider the early-type galaxies. Observations have now revealed that early-type galaxies are composed of both a spherical bulge and an underlying disk (e.g. Emsellem et al. 2007; Graham & Worley 2008; Scott et al. 2014; Laurikainen et al. 2011). The ratio of bulge-to-disk luminosity in typical early-type galaxies is $L_B/L_D \sim 1/3$ (e.g. Graham & Worley 2008; Laurikainen et al. 2011). Thus, for our early-type samples, the potentials can be approximated

by an isothermal density profile for the bulge, combined with a Mestel disk (Binney & Tremaine 1987). Subsequently, integrating over the surface brightness profile yields a mass-dependence of the form M(r) ∝ r. The key features of these potentials is that they have circular velocities given by (Binney & Tremaine 1987):

$$v_c = \frac{GM(r)}{r}, \tag{7}$$

where r is the distance from the centre of the galaxy, and M(r) is the mass distribution within r. The surface brightness is proportional to 1/r in both potentials, hence their sum also scales as 1/r. Subsequently, integrating over the surface brightness profile yields a mass-dependence of the form M(r) ∝ r. From Equation 7, it follows that the circular velocity is independent of r in the combined bulge-disk potential, provided the outer extent of the bulge extends beyond r_h. Beyond the limiting radius of the bulge, it contributes a constant to the total potential, and v_c declines weakly with increasing r. For our sample of late-type galaxies, the potential can, to first-order, be approximated by a simple Mestel disk, for which the circular velocity is independent of r (Binney & Tremaine 1987). Thus, the circular velocity is independent of r in this potential as well. Therefore, in both early- and late-type galaxies, the assumption of a constant circular velocity v_c within the effective radius r_h is a reasonable first-order assumption.

We caution that the potentials of *real* galaxies are considerably more complicated than the assumptions made above suggest. In particular, the ratio M(r)/r drops considerably at small galactocentric radii, roughly where the NSC potential begins to dominate over that of its host. Previous studies have used numerical simulations to model the properties of NSCs formed from GC infall (e.g. Antonini et al. 2012; Antonini 2013), focusing on the final few parsecs. Antonini (2013) found that, after many mergers of GCs with the central NSC, the NSC mass-radius relation steepens from $R_{NSC} \sim M_{NSC}^{0.5}$ to $R_{NSC} \sim M_{NSC}$. Thus, the energy per unit mass in the NSC ends up being independent of the number of accreted GCs, and reaches a roughly constant value. Using more detailed models, Gnedin, Ostriker & Tremaine (2014) found a similarly weak dependence of the form $R_{NSC} \sim M_{NSC}^{0.23}$. Therefore, our results suggest a similarly weak dependence of the galaxy half-mass radius on the total galaxy stellar mass, in order to reproduce the observed relation between the NSC root-mean-square velocity and that of its host. Of equal importance, the circular velocity profiles of real galaxies often are not constant at large galactocentric radii, but instead show considerable fluctuations (e.g. Toloba et al. 2014a,b). Thus, our assumption of a constant circular velocity at all radii is not strictly correct, and is likely the source of much of the scatter seen in Figures 1, 2 and 3.

What else might a linear relation in energy per unit mass be telling us about NSC formation and/or evolution? In particular, we ask: How might a linear relation in energy per unit mass between NSCs and their host galaxies, once in place, be affected by other physical processes characteristic of galaxy formation, such as collisions and mergers occurring in galaxy clusters? Within the framework of the above picture for NSC formation, which should approximately produce NSCs with the same energy per unit mass as their

host, one possible interpretation of this result is that any collisional events affecting the energy per unit mass of the host must have similarly affected its NSC. In other words, significant energy gains or losses cannot have occurred for either the NSC or its host galaxy post-formation. This is because additional energy deposited within NSCs and/or their host galaxies due to direct collisions could contribute to increasing the half-light radius of the system, and hence to decreasing the energy per unit mass (provided the particles involved in the collision are themselves collisionless, which is a decent assumption for stars). This is because the kinetic energies of the colliding galaxies are positive and, via energy conservation, must be added to the total energy per unit mass of the collision/merger product. This contributes to a reduction in the total energy per unit mass of the system (which is a negative quantity for bound systems), which might be observed as an increase in the half-light or effective radius. Thus, if NSC formation involved more energetic collisions than occurred in the host galaxy, this could contribute to a lower root-mean-square velocity in the NSC relative to its host galaxy. Conversely, if galaxy formation involved more energetic collisions than the formation of the central NSC, this could contribute to a lower v_{rms} in the host relative to its central NSC. If the efficiency of either of these scenarios scales with total galaxy mass, then this could contribute to a sub-linear or even super-linear dependence of NSC root-mean-square velocity on host galaxy v_{rms}. In general, collisions that affect the NSC more (or less) than its host contribute to a higher (or lower) energy per unit mass in the host relative to the central NSC, and should increase the scatter in the bottom panels of Figures 1, 2 and 3. The intrinsic scatter in the observed relations is at least consistent with being due in part to different merger histories for the galaxies in our samples.

We caution that the presence of a central SMBH can also strongly affect the evolution and observed structural parameters of NSCs. For example, the presence of a central NSC might be a required pre-cursor to the formation of an SMBH via core collapse (Miller & Davies 2012; Gnedin, Ostriker & Tremaine 2014). Subsequently, the central SMBH can act to disrupt infalling clusters before they reach the nucleus (Antonini et al. 2012; Antonini 2013). Alternatively, a central SMBH or SMBH-SMBH binary could contribute to a higher energy per unit mass in NSCs relative to their hosts, by ejecting stars with a large (positive) energy per unit mass. More work is needed to properly quantify the impact of the presence a central SMBH on the results presented in this paper. Finally, we have also not considered any internal evolution that might occur in NSCs, affecting their structural parameters, nor have we considered energy exchange between an existing NSC and its host galaxy (e.g. Merritt 2013). In general, these omissions are reasonable since the relevant time-scales (e.g. two-body relaxation) tend to exceed a Hubble time in most NSCs (e.g. Merritt 2013).

5.3 Future work

We have argued 1) that NSCs form after their host galaxy bodies, and 2) that, in principle, both formation scenarios for NSC formation discussed above can produce NSCs with the same energy per unit mass as their host galaxies. In

an attempt to identify the most plausible mechanism for NSC formation, we now turn our attention to angular momentum. The general predictions discussed below that arise from consideration of angular momentum could be testable in the future with higher resolution surveys.

What do we expect for the angular momentum content of NSCs relative to their host galaxies? We will argue that, unlike energy per unit mass, the answer could depend on the NSC formation mechanism. In particular, GC orbits form a halo within the host galaxy, with their orbital planes aligned at random angles relative to each other. Thus, if only a single GC inspiral is responsible for forming the NSC, then we would expect significant rotation in the remnant NSC, with the axis of rotation aligned perpendicular to the original orbital plane of the inspiraling GC. This rotation can be canceled by the cumulative effects of many GCs inspiralling into the nucleus, which should create a central NSC with roughly the same energy per unit mass as its host, but nearly zero net angular momentum (within the framework of the picture described above).[4] This is the case for both early- and late-type galaxies. The story changes within the framework of the in situ star formation model for NSC growth. This is because the cumulative effects of galaxy mergers have not depleted the total angular momentum content of late-type galaxies. In late-types, there *is* a preferred plane of accretion for gas, but not for any accreted GCs. Therefore, any in situ star formation occurring in a NSC forming via gas accretion should generally occur in a disk, with its dominant angular momentum vector aligned with that of the host. NSCs formed from many episodes of GC infall, however, should have roughly zero net angular momentum. Thus, we predict that NSCs in late-type galaxies formed primarily via gas accretion and in situ star formation should contain significant angular momentum, which is directly observable as rotation. Naively, this also predicts a correlation between the observed inclination of the host galaxy disk relative to the observer line of sight and the (isophotal) ellipticity of the NSC, with more edge-on disk galaxies having more flattened NSCs. In early-type galaxies, on the other hand, there is no preferred plane of accretion for the gas. Thus, we expect a central NSC with roughly the same energy per unit mass as its host, just as in the GC infall model, but with little to no net angular momentum or rotation.

The implication that NSCs are formed and evolve together with their host galaxies suggests that the origins of NSCs can be distinguished observationally (again, ignoring any internal evolution occuring within the NSCs) when better resolution becomes available. This can be done by decomposing NSCs into bulge and disk components, and comparing the bulge and disk masses, as well as the angle of inclination between the plane of the NSC disk and that of its host galaxy. This is especially true in spiral galaxies, since they have a milder merger history than ellipticals. Consider the quantity $\beta = \cos\theta M_{\mathrm{disk}}/(M_{\mathrm{bulge}}+M_{\mathrm{disk}})$, where M_{disk} is

---

the mass of the disk component, M_{bulge} is the mass of the bugle component and θ is the angle of inclination between the NSC disk and that of its host galaxy. If $\beta \lesssim 0$, then the NSC was formed mainly through GC infall. If, on the other hand, $\beta > 0$ then a non-negligible fraction of the NSC formed through in situ star formation, with $\beta = 1$ corresponding to the case of 0% GC infall and 100% in situ star formation.

6   SUMMARY

We estimate and compare the root-mean-square velocities for a large sample of nuclear star clusters and their host galaxies (both early- and late-type). These are used as proxies for energy per unit mass, and it is demonstrated that NSCs have roughly the same energy per unit mass as their host galaxies, to within an order of magnitude. The origin of this interesting relation is discussed. We interpret this as evidence that NSCs do not form independently of their host galaxies, but rather that their formation and subsequent evolution are coupled. We discuss how our results can potentially be used to offer a clear and observationally testable prediction to distinguish between the different nuclear star cluster formation scenarios, and even quantify their relative contributions.

APPENDIX A: DATA

In this appendix, we present the data used to generate Figures 1, 2 and 3. All calculated NSC and galaxy masses and root-mean-square velocities are summarized in Tables A1, A2 and A3 for each of the late-type, Virgo Cluster and Coma Cluster samples, respectively.

ACKNOWLEDGMENTS

---

[4] In fact, repeated episodes of GC infall may still yield non-negligible rotation in the NSC, provided the orbits characteristic of the bulk of the GC population in the host galaxy exhibit a clear rotation signature, with $v/\sigma > 0.5$. This has been observed in a number of early-type galaxies (e.g. Beasley et al. 2009; Pota et al. 2013), and even the bulge of the Milky Way (e.g. Harris 1996, 2010 update).

REFERENCES

Antonini F., Capuzzo-Dolcetta R., Mastrobuono-Battisti A., Merritt D. 2012, ApJ, 750, 111
Antonini F. 2013, ApJ, 763, 62
Beasley M. A., Cenarro A. J., Strader J., Brodie J. P. 2009, AJ, 137, 5146
Bell E. F., McIntosh D. H., Katz N., Weinberg M. D. 2003, ApJS, 149, 289
Binggeli B., Sandage A., Tarenghi M. 1984, AJ, 89, 64
Binney J., Tremaine S., 1987, Galactic Dynamics (Princeton: Princeton University Press)
Balcells M., Graham A. W., Peletier R. F. 2007, ApJ, 665, 1084
Blakeslee J. P., Lucey J. R., Tonry J. L., Hudson M. J., Narayan V. K., Barris B. J. 2002, MNRAS, 330, 443
Bruzual G., Charlot S. 2003, MNRAS, 344, 1000
Busarello G., Longo G., Feoli A. 1992, A&A, 262, 52

Table A1. Properties of all late-type galaxies. Column 1 gives the object ID. Columns 2 and 3 list the total stellar mass of the galaxy and NSC in units of 10^9 $M_\odot$ and 10^6 $M_\odot$, respectively. Columns 4 and 5 provide the root-mean-square velocities for the galaxy and NSC, respectively, in units of km s^{-1}. The galaxy and NSC mass uncertainties are taken directly from the literature. The uncertainties for the root-mean-square velocities are calculated using the provided uncertainties on both the galaxy or NSC masses and radii, wherever available.

ID	$M_{\rm gal}$ (10^9 $M_\odot$)	$M_{\rm NSC}$ (10^6 $M_\odot$)	$v_{\rm rms,gal}$ (km s^{-1})	$v_{\rm rms,NSC}$ (km s^{-1})
IC0769	$8.761^{0.099}_{-0.098}$	7.963 ± 1.71	78.12 ± 0.7954	69.95 ± 15.02
M108	$0.127^{0.011}_{-0.010}$	1.239 ± 0.266	65.68 ± 3.675	32.65 ± 7.009
MCG-01-03-085	$0.658^{0.013}_{-0.013}$	2.417 ± 0.4541	42.96 ± 0.8615	42.34 ± 7.954
NGC0428	$2.661^{0.151}_{-0.143}$	3.619 ± 1.297	63.53 ± 3.214	80.54 ± 28.87
NGC0600	$6.232^{0.051}_{-0.051}$	2.595 ± 0.6061	68.75 ± 0.5458	65.52 ± 15.3
NGC0853	$2.691^{0.021}_{-0.021}$	2.692 ± 0.6289	69.64 ± 0.6369	52.51 ± 12.26
NGC0864	$9.07^{0.451}_{-0.430}$	78.0 ± 2.024	105.1 ± 4.838	249.3 ± 6.466
NGC1042	$0.253^{0.070}_{-0.055}$	4.432 ± 3.346	35.41 ± 11.38	85.62 ± 64.64
NGC2500	$0.800^{0.030}_{-0.029}$	0.8753 ± 0.2416	39.13 ± 1.374	19.6 ± 5.41
NGC2541	$0.643^{0.027}_{-0.026}$	0.6041 ± 0.1297	41.26 ± 1.527	36.04 ± 7.738
NGC2552	$0.270^{0.021}_{-0.019}$	3.549 ± 0.8097	24.06 ± 1.237	87.37 ± 19.93
NGC2805	$6.314^{0.120}_{-0.118}$	9.509 ± 2.169	77.24 ± 1.515	103.7 ± 23.67
NGC3041	$15.17^{0.677}_{-0.648}$	15.15 ± 6.995	105.9 ± 4.083	56.52 ± 26.09
NGC3259	$13.23^{0.085}_{-0.085}$	20.56 ± 4.327	136.6 ± 0.8513	72.56 ± 15.27
NGC3274	$0.681^{0.023}_{-0.023}$	0.4157 ± 0.0390	47.78 ± 2.064	24.41 ± 2.293
NGC3319	$1.036^{0.014}_{-0.014}$	1.759 ± 0.2793	45.37 ± 0.688	28.37 ± 4.505
NGC3338	$19.23^{0.455}_{-0.444}$	263.9 ± 27.08	138.3 ± 3.337	198.5 ± 20.37
NGC3346	$6.142^{0.055}_{-0.055}$	3.091 ± 0.722	72.56 ± 0.4986	77.74 ± 18.16
NGC3359	$13.88^{0.043}_{-0.043}$	9.465 ± 1.153	101.1 ± 0.2946	54.31 ± 6.618
NGC3423	$2.263^{0.029}_{-0.029}$	1.791 ± 0.1636	70.02 ± 0.9634	41.84 ± 3.823
NGC3445	$1.736^{0.009}_{-0.009}$	3.751 ± 0.8557	60.51 ± 0.2824	75.91 ± 17.32
NGC3455	$7.435^{0.049}_{-0.049}$	8.111 ± 1.741	91.52 ± 0.5246	89.05 ± 19.12
NGC3666	$9.215^{0.063}_{-0.063}$	48.36 ± 28.98	125.6 ± 0.9413	104.1 ± 62.37
NGC3756	$21.71^{0.119}_{-0.118}$	30.35 ± 16.53	120.7 ± 0.5633	158.4 ± 86.31
NGC3913	$2.046^{0.018}_{-0.018}$	1.314 ± 0.3015	58.8 ± 0.6037	10.67 ± 2.45
NGC3949	$14.53^{0.017}_{-0.017}$	7.723 ± 1.765	142.9 ± 0.1635	101.9 ± 23.29
NGC4030	$43.76^{1.497}_{-1.447}$	284.0 ± 14.45	283.4 ± 10.26	268.1 ± 13.64
NGC4041	$29.84^{0.050}_{-0.050}$	78.82 ± 46.31	220.6 ± 0.4428	93.96 ± 55.21
NGC4062	$13.98^{0.025}_{-0.025}$	3.229 ± 0.6933	131.7 ± 0.2014	52.71 ± 11.32
NGC4096	$7.449^{0.104}_{-0.103}$	1.397 ± 0.2999	108.5 ± 1.624	32.75 ± 7.032
NGC4204	$0.182^{0.006}_{-0.006}$	0.1915 ± 0.0447	22.89 ± 0.7458	21.39 ± 4.996
NGC4208	$15.57^{0.057}_{-0.057}$	8.812 ± 1.892	$141. \pm 0.4547$	39.25 ± 8.427
NGC4237	$24.37^{0.085}_{-0.085}$	14.15 ± 2.209	174.5 ± 0.5642	68.42 ± 10.68
NGC4393	$0.001^{0.002}_{-0.000}$	0.4048 ± 0.0819	$3.289 \pm 136.$	19.05 ± 3.852
NGC4395	$0.013^{0.001}_{-0.001}$	3.203 ± 0.6301	11.53 ± 1.301	67.77 ± 13.33
NGC4411b	$0.684^{0.015}_{-0.015}$	4.766 ± 1.087	38.07 ± 0.7635	46.21 ± 10.54
NGC4498	$0.013^{0.003}_{-0.002}$	1.726 ± 0.3706	25.77 ± 3.636	34.06 ± 7.313
NGC4517	$0.012^{0.003}_{-0.002}$	0.8894 ± 0.1909	27.99 ± 4.157	28.84 ± 6.191
NGC4522	$6.07^{0.063}_{-0.063}$	1.679 ± 0.3605	77.42 ± 1.023	17.49 ± 3.756
NGC4525	$3.307^{0.018}_{-0.018}$	1.745 ± 0.3451	66.77 ± 0.3455	64.58 ± 12.77
NGC4534	$1.079^{0.014}_{-0.014}$	0.8319 ± 0.1557	46.78 ± 0.5342	20.89 ± 3.91
NGC4567	$0.604^{0.018}_{-0.017}$	55.6 ± 11.7	106.8 ± 2.657	238.6 ± 50.21
NGC4571	$6.938^{0.103}_{-0.101}$	7.449 ± 0.1933	91.27 ± 1.382	83.46 ± 2.165
NGC4592	$1.69^{0.007}_{-0.007}$	0.8037 ± 0.1725	56.28 ± 0.2334	39.64 ± 8.51
NGC4618	$1.507^{0.010}_{-0.010}$	0.4788 ± 0.2468	62.28 ± 0.3859	15.66 ± 8.069
NGC4625	$0.957^{0.004}_{-0.004}$	1.772 ± 0.0599	58.72 ± 0.2616	20.69 ± 0.699
NGC4631	$0.006^{0.001}_{-0.001}$	0.8037 ± 0.1691	21.62 ± 2.386	17.57 ± 3.696
NGC4635	$1.937^{0.035}_{-0.035}$	4.488 ± 1.668	48.05 ± 0.719	47.38 ± 17.61
NGC4651	$67.51^{0.199}_{-0.199}$	$404.8 \pm 93210000.$	251.2 ± 0.721	$172.1 \pm 39620000.$
NGC4701	$7.094^{0.044}_{-0.044}$	53.23 ± 12.14	114.9 ± 0.665	218.4 ± 49.82
NGC4900	$11.55^{0.707}_{-0.666}$	18.59 ± 0.6053	106.4 ± 5.072	113.6 ± 3.698
NGC4904	$5.951^{0.055}_{-0.054}$	2.281 ± 0.5328	95.14 ± 0.857	44.3 ± 10.35
NGC5112	$2.633^{0.097}_{-0.094}$	1.41 ± 0.0859	50.58 ± 1.697	21.43 ± 1.306
NGC5204	$0.324^{0.004}_{-0.004}$	0.2335 ± 0.0153	34.09 ± 0.4149	35.43 ± 2.32
NGC5300	$4.591^{0.203}_{-0.195}$	15.03 ± 0.5514	68.9 ± 2.784	39.61 ± 1.453
NGC5334	$21.76^{0.218}_{-0.216}$	8.635 ± 0.716	93.79 ± 0.77	39.5 ± 3.276
NGC5585	$0.799^{0.017}_{-0.016}$	0.8341 ± 0.1325	47.78 ± 0.964	34.58 ± 5.492
NGC5668	$3.452^{0.308}_{-0.283}$	4.066 ± 0.6458	71.93 ± 5.838	54.91 ± 8.721
NGC5964	$0.018^{0.004}_{-0.004}$	3.648 ± 0.4912	20.7 ± 2.778	57.18 ± 7.698
NGC5970	$0.592^{0.056}_{-0.051}$	8.186 ± 1.758	114.2 ± 6.918	33.59 ± 7.212

Table A2. Properties of all Virgo Cluster galaxies. The columns are the same as in Table A1.

ID	M_{gal} $(10^9\ M_\odot)$	M_{NSC} $(10^6\ M_\odot)$	$v_{rms,gal}$ $(km\ s^{-1})$	$v_{rms,NSC}$ $(km\ s^{-1})$
VCC1720	20.21 ± 5.31	89.24 ± 3.371	142.9 ± 37.55	158.5 ± 14.36
VCC1883	16.66 ± 3.92	25.12 ± 0.949	143.4 ± 33.73	167.7 ± 49.31
VCC1242	15.27 ± 3.17	23.14 ± 0.8741	168.1 ± 34.91	133.2 ± 27.12
VCC784	16.79 ± 3.14	63.61 ± 2.403	210.1 ± 39.29	111.1 ± 6.401
VCC828	13.69 ± 3.00	104.4 ± 3.942	176.3 ± 38.64	102. ± 5.162
VCC1250	3.68 ± 2.04	21.48 ± 0.8115	96.18 ± 53.32	145.9 ± 39.67
VCC1125	8.06 ± 3.4	3.814 ± 0.144	149.3 ± 62.98	41.31 ± 5.066
VCC1283	9.08 ± 1.79	8.99 ± 0.3396	120. ± 23.66	67.49 ± 9.271
VCC1261	4.87 ± 1.69	14.25 ± 0.5383	86.41 ± 29.99	103.1 ± 20.42
VCC698	9.52 ± 2.56	11.33 ± 0.4278	139. ± 37.39	86.12 ± 15.06
VCC1422	3.82 ± 1.35	7.342 ± 0.2773	73.24 ± 25.88	75.05 ± 15.28
VCC2048	2.94 ± 1.08	2.105 ± 0.0795	84.73 ± 31.12	42.7 ± 9.777
VCC1871	2.26 ± 0.58	24.18 ± 0.9134	106.3 ± 27.29	82.14 ± 6.162
VCC1910	2.1 ± 0.81	10.1 ± 0.3814	73.46 ± 28.34	84.47 ± 15.88
VCC856	2.22 ± 0.85	19.66 ± 0.7427	64.05 ± 24.53	58.74 ± 3.485
VCC140	2.33 ± 0.71	0.7763 ± 0.0293	88.08 ± 26.84	30.78 ± 9.863
VCC1355	1.82 ± 0.35	2.38 ± 0.0899	42.9 ± 8.25	41.01 ± 7.712
VCC1087	3.29 ± 1.07	8.816 ± 0.333	70.6 ± 22.96	93.64 ± 24.53
VCC1861	2.88 ± 1.00	6.08 ± 0.2296	69.81 ± 24.24	37.04 ± 2.589
VCC543	2.19 ± 0.65	1.074 ± 0.0406	60.79 ± 18.04	12.13 ± 0.631
VCC1431	2.2 ± 0.74	10.49 ± 0.3963	82.82 ± 27.86	34.77 ± 1.678
VCC1528	1.63 ± 0.48	0.7213 ± 0.0272	71.36 ± 21.01	32.8 ± 12.82
VCC1695	1.69 ± 0.78	1.06 ± 0.0400	43.91 ± 20.27	34.44 ± 10.13
VCC437	2.8 ± 1.25	6.18 ± 0.2334	57.66 ± 25.74	44.71 ± 4.132
VCC2019	1.02 ± 0.72	5.671 ± 0.2142	40.64 ± 28.69	72.46 ± 17.7
VCC33	0.43 ± 0.25	0.7211 ± 0.0272	38.06 ± 22.13	24.6 ± 5.461
VCC200	1.34 ± 0.49	0.392 ± 0.0148	56.15 ± 20.53	16.64 ± 3.13
VCC1488	0.41 ± 0.38	0.1285 ± 0.0049	34.72 ± 32.18	11.75 ± 3.319
VCC1895	0.76 ± 0.39	0.2053 ± 0.0078	47.42 ± 24.34	16.2 ± 5.435
VCC1545	1.41 ± 0.42	1.146 ± 0.0433	63.66 ± 18.96	28.84 ± 5.563
VCC1192	1.85 ± 0.62	19.78 ± 0.747	89.74 ± 30.08	66.25 ± 4.577
VCC1075	1.11 ± 0.47	2.178 ± 0.0823	43.87 ± 18.58	38.73 ± 7.103
VCC1627	1.03 ± 0.32	38.08 ± 1.438	90.63 ± 28.16	72.04 ± 3.736
VCC1440	1.19 ± 0.44	14. ± 0.5287	69.07 ± 25.54	81.93 ± 10.7
VCC230	0.69 ± 0.29	5.445 ± 0.2057	48.38 ± 20.33	66.56 ± 14.34
VCC2050	0.29 ± 0.26	0.6627 ± 0.0250	27.61 ± 24.76	16.42 ± 1.849
VCC751	1.41 ± 0.51	2.203 ± 0.0832	57.9 ± 20.94	41.12 ± 8.369
VCC1828	1.26 ± 0.47	1.567 ± 0.0592	48.56 ± 18.11	27.17 ± 3.491
VCC538	0.63 ± 0.26	2.382 ± 0.0900	63.25 ± 26.1	46.17 ± 10.91
VCC1407	1.24 ± 0.42	4.252 ± 0.1606	59.28 ± 20.08	29.98 ± 2.003
VCC1886	0.51 ± 0.1	0.9599 ± 0.0363	34.27 ± 6.72	25.07 ± 4.384
VCC1199	0.58 ± 0.16	14.29 ± 0.5396	73.43 ± 20.26	78.03 ± 9.158
VCC1539	0.52 ± 0.11	3.209 ± 0.1212	26.78 ± 5.665	18.03 ± 0.831
VCC1185	0.89 ± 0.51	2.6 ± 0.0982	36.03 ± 20.65	37.36 ± 5.418
VCC1826	0.61 ± 0.22	7.802 ± 0.2947	52.35 ± 18.88	91.54 ± 25.86
VCC1489	0.32 ± 0.06	0.5612 ± 0.0212	29.84 ± 5.596	16.12 ± 2.038
VCC1661	0.43 ± 0.08	5.142 ± 0.1942	18.38 ± 3.42	41.03 ± 3.83

Cappellari M. et al. 2006, MNRAS, 366, 1126

Cappellari M., Scott N., Alatalo K., Blitz L., Bois M., Bournaud F., Bureau M., Crocker A. F., Davies R. L., Davis T. A., de Zeeuw P. T., Duc P.-A., Emsellem E., Khochfar S., Krajnovic D., Kuntschner H., McDermind R. M., Morganti R., Naab T., Oosterloo T., Sarzi M., Serra P., Weijmans A.-M., Young L. M. 2013a, MNRAS, 432, 1709

Cappellari M., McDermind R. M., Alatalo K., Blitz L., Bois M., Bournaud F., Bureau M., Crocker A. F., Davies R. L., Davis T. A., de Zeeuw P. T., Duc P.-A., Emsellem E., Khochfar S., Krajnovic D., Kuntschner H., Morganti

R., Naab T., Oosterloo T., Sarzi M., Scott N., Serra P., Weijmans A.-M., Young L. M. 2013b, MNRAS, 432, 1862

Capuzzo-Dolcetta R., Miocchi P. 2008, MNRAS, 388, 69

Carter D., et al. 2008, ApJS, 176, 424

Chae K.-H., Bernardi M., Kravstov A. V. 2014, MNRAS, in press (arXiv:1305.5471)

Cote P., Blakeslee J. P., Ferrarese L., Jordan A., Mei S., Merritt D., Milosavljevic M., Peng E. W., Tonry J. L., West M. J. 2004, ApJS, 153, 223

Cote P., Piatek S., Ferrarese L., Jordan A., Merritt D., Peng E. W., Hasegan M., Blakeslee J. P., Mei S., West M. J., Milosavljevic M., Tonry J. L. 2006, ApJS, 165, 57

Table A3. Properties of all Coma Cluster galaxies. The columns are the same as in Table A1. Uncertainties on the NSC masses are provided when available.

ID	M_{gal} $(10^9 \ M_\odot)$	M_{NSC} $(10^6 \ M_\odot)$	$v_{rms,gal}$ $(km \ s^{-1})$	$v_{rms,NSC}$ $(km \ s^{-1})$
LEDA126789	2.339 ± 0.021	$12.28 \pm -$	79.96 ± 0.19	30.76 ± 1.10
SDSSJ125950.18-275445.4	2.133 ± 0.019	$8.492 \pm -$	57.47 ± 0.20	37.2 ± 1.69
SDSSJ130007.12-275551.4	1.476 ± 0.013	$25.65 \pm -$	73.16 ± 0.52	48.86 ± 1.48
SDSSJ125926.45-275124.7	1.346 ± 0.012	2.812 ± 0.259	58.06 ± 0.29	20.71 ± 2.35
SDSSJ130026.16-280032.0	1.12 ± 0.010	$8.492 \pm -$	47.36 ± 0.29	40.03 ± 1.40
SDSSJ125914.43-280217.3	0.162 ± 0.006	$3.707 \pm -$	16.2 ± 0.43	21.1 ± 1.42
SDSSJ125953.93-275813.7	1.476 ± 0.013	$9.312 \pm -$	55.6 ± 0.17	32.9 ± 1.25
SDSSJ125636.78-271247.8	1.618 ± 0.028	$3.707 \pm -$	40.25 ± 0.60	28.97 ± 3.05
SDSSJ130000.97-275929.5	1.021 ± 0.009	$21.33 \pm -$	47.33 ± 0.30	54.4 ± 1.40
SDSSJ125844.58-274458.2	1.476 ± 0.013	$17.74 \pm -$	44.28 ± 0.10	39.71 ± 1.15
SDSSJ130042.86-280313.8	0.849 ± 0.007	$2.339 \pm -$	34.21 ± 0.19	23.51 ± 2.84
COMAi125949.960p275433	0.588 ± 0.005	$10.21 \pm -$	43.51 ± 0.30	37.28 ± 1.42
SDSSJ130032.61-280331.4	0.706 ± 0.012	$11.2 \pm -$	30.2 ± 0.52	39.41 ± 1.27
SDSSJ130036.58-275552.2	0.588 ± 0.005	$4.887 \pm -$	36.76 ± 0.31	31.79 ± 2.14
COMAi125713.240p272437	0.588 ± 0.005	$7.064 \pm -$	37.44 ± 0.18	30.16 ± 1.26
SDSSJ125942.36-280158.5	0.644 ± 0.011	$5.358 \pm -$	31.93 ± 0.42	20.43 ± 0.96
SDSSJ130027.57-280323.9	0.536 ± 0.009	$1.618 \pm -$	25.91 ± 0.40	17.55 ± 1.86
SDSSJ130004.03-280030.7	0.489 ± 0.004	$7.064 \pm -$	36.71 ± 0.43	33.8 ± 1.53
SDSSJ125902.43-280021.3	0.407 ± 0.004	$5.875 \pm -$	36.47 ± 0.27	29.62 ± 1.64
SDSSJ130018.70-275512.6	0.371 ± 0.003	$4.065 \pm -$	31.06 ± 0.22	29.42 ± 1.45
SDSSJ130044.10-280215.4	0.536 ± 0.009	$5.875 \pm -$	25.56 ± 0.47	28.55 ± 1.10
SDSSJ125943.53-275620.6	0.371 ± 0.010	$9.312 \pm -$	26.72 ± 0.54	42.67 ± 1.55
COMAi125828.358p271315	0.489 ± 0.009	$3.381 \pm -$	27.16 ± 0.33	24.12 ± 1.35
SDSSJ130042.51-280325.4	0.338 ± 0.006	$7.745 \pm -$	32.48 ± 0.53	27.71 ± 0.89
SDSSJ130037.30-275441.0	0.338 ± 0.009	$8.492 \pm -$	27.2 ± 0.68	38.22 ± 1.53
SDSSJ125955.93-275748.6	0.281 ± 0.002	$2.565 \pm -$	25.61 ± 0.30	16.91 ± 1.31
SDSSJ130032.96-275406.6	0.536 ± 0.009	$11.2 \pm -$	21.68 ± 0.42	39.41 ± 1.27
SDSSJ130003.18-275648.3	0.148 ± 0.003	1.476 ± 0.413	18.94 ± 0.28	15.75 ± 2.95
SDSSJ125927.22-275257.0	0.195 ± 0.003	$5.875 \pm -$	21.92 ± 0.30	18.71 ± 0.62
SDSSJ125951.46-275935.4	0.213 ± 0.004	$3.707 \pm -$	23.99 ± 0.33	24.04 ± 1.22
SDSSJ125930.83-275810.2	0.234 ± 0.014	$7.745 \pm -$	23.96 ± 1.30	35.52 ± 1.35
SDSSJ125945.55-280313.4	0.162 ± 0.007	$3.381 \pm -$	17.93 ± 0.56	17.78 ± 1.31
COMAi13035.990p275505.4	0.162 ± 0.003	$2.565 \pm -$	18.36 ± 0.31	22.19 ± 2.18
SDSSJ130024.85-27.99085	0.162 ± 0.004	$6.442 \pm -$	20.25 ± 0.46	31.02 ± 1.29
SDSSJ125853.08-274741.8	0.234 ± 0.008	$3.083 \pm -$	22.85 ± 0.61	22.94 ± 1.46
SDSSJ125708.35-272923.9	0.148 ± 0.005	$5.875 \pm -$	22.63 ± 0.75	31.06 ± 1.42
SDSSJ125959.08-275841.4	0.281 ± 0.007	$11.2 \pm -$	18.53 ± 0.62	43.89 ± 1.40
SDSSJ130030.94-280312.8	0.085 ± 0.004	$3.707 \pm -$	14.98 ± 0.65	24.3 ± 1.44
SDSSJ130030.94-280312.8	0.093 ± 0.005	$3.707 \pm -$	14.86 ± 0.76	23.13 ± 1.24
COMAi125937.351p28210.6	0.085 ± 0.003	1.618 ± 0.149	17.2 ± 0.59	14.02 ± 1.66
SDSSJ130034.32-275817.6	0.093 ± 0.002	1.476 ± 0.136	16.91 ± 0.30	$15. \pm 1.81$
SDSSJ125934.39-275942.9	0.148 ± 0.004	$1.945 \pm -$	19.09 ± 0.46	16.17 ± 1.31
SDSSJ130039.32-275748.4	0.093 ± 0.003	$2.133 \pm -$	14.9 ± 0.43	16.88 ± 1.15
COMAi13039.554p275350.0	0.123 ± 0.003	$2.565 \pm -$	17.57 ± 0.49	22.92 ± 2.18
SDSSJ125951.81-275726.3	0.135 ± 0.012	$5.875 \pm -$	15.34 ± 1.44	31.18 ± 1.68
COMAi125925.477p28211.0	0.071 ± 0.006	1.476 ± 0.136	13.8 ± 0.97	11.72 ± 2.03
SDSSJ125700.89-273155.1	0.102 ± 0.011	$2.339 \pm -$	11.54 ± 0.88	21.01 ± 1.47
SDSSJ130030.94-280312.8	0.085 ± 0.004	$3.707 \pm -$	14.98 ± 0.65	24.3 ± 1.44
SDSSJ130030.94-280312.8	0.093 ± 0.005	$3.707 \pm -$	14.86 ± 0.76	23.13 ± 1.24
SDSSJ130029.81-280401.0	0.085 ± 0.002	1.021 ± 0.094	14.54 ± 0.31	12.18 ± 1.81
SDSSJ130004.04-275342.7	0.281 ± 0.015	$5.875 \pm -$	14.38 ± 0.72	30.94 ± 1.41
SDSSJ125952.18-275946.3	0.078 ± 0.002	1.228 ± 0.113	15.05 ± 0.40	15.15 ± 2.24
SDSSJ125856.78-274644.5	0.049 ± 0.001	0.234 ± 0.088	13.76 ± 0.31	3.34 ± 2.08

den Brok M., et al. 2014, MNRAS, 445, 2385

Emsellem E., Cappellari M., Krajnovic D., van de Ven G., Bacon R., Bureau M., Davies R. L., de Zeeuw P. T., Falcon-Barroso J., Kuntschner H. 2007, MNRAS, 379, 401

Gnedin O. Y., Ostriker J. P., Tremaine S. 2014, ApJ, 785, 71

Graham A. W., Driver S. P., Petrosian V., Conselice C. J., Bershady M. A., Crawford S. M., Goto T. 2005, AJ, 130, 1535

Ferrarese L., Cote P., Jordan A., Peng E. W., Blakeslee J. P., Piatek S., Mei S., Merritt D., Milosavljevic M., Tonry J. L., West M. J. 2006, ApJS, 164, 334

Forbes D. A., Lasky P., Graham A. W., Spitler L. 2008, MNRAS, 389, 1924

Georgiev I. Y., Böker T. 2014, arXiv:1404.5956

Graham A. W., Worley. C. C. 2008, MNRAS, 388, 1708

Graham A. W., Spitler L. R. 2009, MNRAS, 397, 2148

Graham A. W. 2012, MNRAS, 422, 1586

Harris, W. E. 1996, AJ, 112, 1487 (2010 update)

Hartmann M., Debattista V. P., Seth A., Cappellari M., Quinn T. R. 2011, MNRAS, 418, 2697

Jaffe W. 1983, MNRAS, 202, 995

Jeffreys H. 1946, RSPSA, 186, 453

Jordan A., McLaughlin D. E., Cote P., Ferrarese L., Peng E. W., Mei S., Villegas D., Merritt D., Tonry J. L., West M. J. 2007, ApJS, 171, 101

Kormendy J., Kennicutt R. C. Jr. 2004, ARA&A, 42, 603

Kroupa P. 2001, MNRAS, 322, 231

Laurikainen E., Salo H., Buta R., Knapen J. H. 2011, MN-RAS, 418, 1452

Leigh N. W. C., Böker T., Knigge C. 2012, MNRAS, 424, 2130

Long K. S., Charles P. A., Dubus G., 2002, ApJ, 569, 204

McLaughlin D. E., King A. R., Nayakshin S. 2006, ApJL, 650, L37

Merritt D. 2013, Dynamics and Evolution of Galactic Nuclei (Princeton: Princeton University Press)

Miller M. C., Davies M. B. 2012, ApJ, 755, 81

Nayakshin S., Wilkinson M. I., King A. 2009, MNRAS, 398, 54

Nguyen D. D., Seth A. C., Reines A. E., den Brok M., Sand D., McLeod B. 2014, ApJ, 794, 34

Pota V., Forbes D. A., Romanowsky A. J., Brodie J. P., Spitler L. R., Strader J., Foster C., Arnold J. A., Benson A., Blom C., Hargis J. R., Rhode K. L., Usher C. 2013, MNRAS, 428, 389

Quinlan G. D., Shapiro S. L. 1990, ApJ, 356, 483

Scott N., Graham A. W. 2013, ApJ, 763, 76

Scott N., Davies R. L., Houghton R. C. W., Cappellari M., Graham A. W., Pimbblet K. A. 2014, MNRAS, 441, 274

Seth A., Agueros M., Lee D., Basu-Zych A. 2008, ApJ, 678, 116

Spitzer L. Jr. 1969, ApJL, 158, L139

Toloba E., Guhathakurta P., Peletier R., Boselli A., Lisker T., Falcon-Barroso J., Simon J., van de Ven G., Paudel S., Emsellem E., Janz J., den Brok M., Gorgas J., Hensler G., Laurikainen E., Niemi S. M., Rys A., Salo H. 2014, ApJS, accepted (arXiv:1410.1550)

Toloba E., Guhathakurta P., Boselli A., Peletier R., Emsellem E., Lisker T., van de Ven G., Simon J., Falcon-Barroso J., Adams J., Benson A., Boissier S., den Brok M., Gorgas J., Hensler G., Janz J., Laurikainen E., Paudel S., Rys A., Salo H. 2014, ApJ, submitted (arXiv:1410.1552)

Tonry J. L., Dressler A., Blakeslee J. P., Ajhar E. A., Fletcher A. B., Luppino G. A., Metzger M. R. 2001, ApJ, 546, 681

Tremaine S. D., Ostriker J. P., Spitzer L. Jr. 1975, ApJ, 196, 407

Watson L. C., Martini P., Lisenfeld U., Wong M.-H., Böker T., Schinnerer E. 2005, ApJ, 751, 123

This paper has been typeset from a TeX/ LaTeX file prepared by the author.